IEEE Access
Multidisciplinary ⋮ Rapid Review ⋮ Open Access Journal

Received 26 March 2024, accepted 3 May 2024, date of publication 9 May 2024, date of current version 17 May 2024.

Digital Object Identifier 10.1109/ACCESS.2024.3399034

RESEARCH ARTICLE

Rodent Transcranial Magnetic Stimulation Coil Structure With Controllable Induction Electric Field Direction

JIAYU ZHAI[1], JINTING WANG[1], HAO CUI[1], QIMING CHEN[2], (Member, IEEE), JIUGE LIN[1], DONGHUA PAN[1,2], (Member, IEEE), AND LIYI LI[1,2], (Member, IEEE)

[1]Department of Electrical Engineering, Harbin Institute of Technology, Harbin 150001, China
[2]Laboratory for Space Environment and Physical Sciences, Harbin Institute of Technology, Harbin 150001, China

Corresponding author: Donghua Pan (pandonghua@hit.edu.cn)

This work was supported in part by the National Key Research and Development Program of China under Grant 2022YFA1604500, and in part by the National Natural Science Foundation of China under Grant 52077040.

ABSTRACT Animal transcranial magnetic stimulation (TMS) research is meaningful for exploring the mechanism of TMS and promoting the clinical promotion of new therapeutic methods. Tracing back the physiological phenomena caused by TMS is limited by the spatial resolution of the induced electric field. Through human and animal experiments, life science has proven that electric field direction affects the effect of magnetic stimulation, but this factor has not been introduced into the design of animal TMS coils. Therefore, this paper aims to design the TMS coil (EC-X) with controllable induced electric field direction, by finding the most favorable electric field direction for target activation, which can reduce interference to non-target areas and improve stimulation accuracy and energy utilization. Firstly, the structure of EC-X is proposed, establishing the Electromagnetic field Analytical Calculation Model (EM-ACM) for the arbitrarily shaped coil in the air domain, it is theoretically proven that EC-X can achieve direction control of the electric field. Then, the coil structure (such as coil length and angle) is optimized based on maximum ampere-turn AN_{max} and stimulation focusing degree F_c. Finally, the measurement of xy plane magnetic field distribution proves the accuracy of EM-ACM calculation results, which indirectly proves the feasibility of EC-X. Compared with the Figure-8 coil, EC-X can change the planar electric field direction without moving the coil, which has potential application value.

INDEX TERMS Coil, controllable induced electric field direction, transcranial magnetic stimulation.

I. INTRODUCTION

Transcranial Magnetic Stimulation (TMS) uses short strong current pulse to excite a rapidly changing magnetic field, which generates induced electric field in biological tissue, then changes the cell membrane potential, and finally regulates neural activity. It has been used in Alzheimer's disease, Epilepsy, Parkinson's disease, and so on. However, the mechanism of induced electric field on neurons and how its derivative effects propagate in the brain are still unknown [1]. Due to potential safety and ethical problems, it is impossible to reveal the biophysical mechanism of TMS through human experiments, animal TMS research is essential.

The key to translating animal TMS findings to human TMS is first reproducing similar brain stimulation effects on animal models. Human TMS stimulation usually uses the Figure-8 coil, and the suprathreshold stimulation depth is about 1.5cm [2]. The average size of the adult rat brain is about $0.6cm^3$ [3], directly using human coil will cause diffuse stimulation of the rat brain, and the spatial resolution of the induced electric field cannot meet the research needs. To this end, researchers have launched research on rodent-specific magnetic stimulation coil.

The associate editor coordinating the review of this manuscript and approving it for publication was Yi Ren.

When designing for the rodents, one way to improve the accuracy of magnetic stimulation is to miniaturize the commonly used TMS coils in humans. In 2001, Andreas et al. [4] used the commercially available Figure-8 coil of 5cm to measure the Motor Evoked Potential (MEP) of rats, the experimental results can only characterize the overall excitability of the corticospinal cord. Rotenberg et al. [5] placed the Figure-8 coil laterally to stimulate anesthetized rats and observed unilateral brachioradialis muscle activation in 2010, but they only attributed the generation of MEP to the unilateral hemisphere and could not explain the specific cortical origin. The above physiological experiments indicate that the spatial range of effective stimulation generated by the coil is still large.

Wrapping ferromagnetic materials to converge the local magnetic field becomes another idea to enhance the focus of stimulation. Tang et al. [6] proposed the cylindrical coil wrapped around an iron core, and the electric field intensity below the coil is about 10V/m, stimulating the motor cortex of anesthetized rats can observe a significant increase in MEP amplitude. Khokhar et al. [7] optimized the cylindrical coil to be tapered, the frequency of spontaneous population events in extracorporeal mouse brain slices significantly decreased after coil stimulation. Takahiro et al. [8] further reduced the coil size to 4mm, allowing in vivo auditory cortical stimulation. In addition, some researchers have improved stimulation focus and electric field intensity by combining the Halo coil with circular [9] or Figure-8 coil [10].

The above coils are all valuable efforts to promote the development of animal-specific TMS coil, but most of them are suboptimal designs based on human coil structure, either through experience or simple exploratory combinations, neglecting the electric field direction when designing the coil. Human clinical data indicates [11] that the optimal stimulation effect occurs when the angle of the Figure-8 coil handle to the longitudinal cerebral fissure is 45°. To ascertain each person's Motor Threshold (MT), the coil must be adjusted multiple times. In 2009, through the homogeneous mouse MRI model, Salvador et al. [12] found that under the same excitation, the activation thresholds of Figure-8 and the circular coil are different when they are in different positions relative to the target. The team [13] established a simplified model of cerebral cortical sulcus gyrus in 2011, simulated Figure-8 coil to stimulate different types of cells in different locations, and found cell depolarization sites and thresholds were different. In general, both human and animal experiments indicate that the effect of TMS stimulation is sensitive to the electric field direction.

In view of the fact that the previous animal coil design does not consider the induced electric field direction which affects the stimulation effect, this paper aims to propose a new coil structure that allows for control of the induced electric field direction, the relative direction between the induced electric field and the stimulus target can be flexibly adjusted without changing the coil position. By finding the most favorable electric field direction for target activation, interference with non-target areas can be reduced, which is expected to improve the accuracy of stimulation and reduce the energy required for effective stimulation.

The main contents of this paper are as follows: in II, introduce the coil EC-X with the controllable direction of the induced electric field, and the feasibility is verified by the established Electromagnetic field Analytical Calculation Model (EM-ACM). Then, prove the performance advantages of EC-X by comparing the induced electric field direction generated by EC-4 and Figure-8 in the plane below them. In III, optimize the coil geometric parameters (such as coil length and angle) to improve the stimulation efficiency. In IV, make the coil physical object and set up the platform to measure the xy plane magnetic field distribution, indirectly proving through experiments that EC-X can achieve controllable electric field direction.

II. ELECTRIC FIELD DIRECTION CONTROLLABLE COIL

A. ELECTROMAGNETIC FIELD ANALYTICAL CALCULATION MODEL

The magnetic permeability of biological tissue is uniform, the magnetic field generated by time-varying current reaches the target area almost without attenuation, and the induced electric field generated follows Faraday's electromagnetic law:

$$\nabla \times \boldsymbol{E} = -\frac{\partial \boldsymbol{B}}{\partial t} \tag{1}$$

Magnetic induction intensity $\boldsymbol{B}$ is the curl of magnetic vector potential $\boldsymbol{A}$, satisfying (2):

$$\boldsymbol{B} = \nabla \times \boldsymbol{A} \tag{2}$$

ϕ is the electric scalar potential, $\boldsymbol{E}$ follows the expression:

$$\boldsymbol{E} = -\frac{\partial \boldsymbol{A}}{\partial t} - \nabla\phi \tag{3}$$

The former is the primary field caused by the change of magnetic field, and the latter is the secondary field caused by charge accumulation in the boundary layer due to different tissue conductivity [14]. This paper mainly analyzes the electromagnetic field distribution in the air domain, and the influence of secondary fields can be ignored.

The boundary conditions in the air domain are relatively simple, and the spatial electromagnetic field distribution can be calculated directly. An empty core coil can be equivalent to multiple connected energized segments, the effect of each energized segment on the observation point is superimposed, thereby establishing the Electromagnetic field Analytical Calculation Model (EM-ACM) of any shape coil in the air domain. For any point Q in space, $d\boldsymbol{B}$ produced by the current element $\boldsymbol{I}d\boldsymbol{l}$ in the energized segment satisfies Biot-Savart law:

$$d\boldsymbol{B} = \frac{\mu_0}{4\pi}\frac{I d\boldsymbol{l} \times \boldsymbol{r}}{r^3} \tag{4}$$

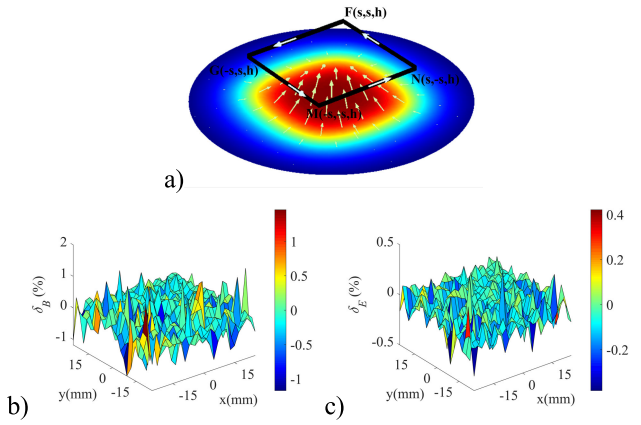

FIGURE 1. a). Square coil magnetic field distribution. The white arrow represents the coil current and the yellow arrow represents $\boldsymbol{B}$. b). δ_B. c). δ_E. b) and c) represent the error between the EM-ACM calculation and the COMSOL simulation.

$\boldsymbol{Idl}$ position coordinate is (x, y, z), and $\boldsymbol{r}$ is the vector that $\boldsymbol{Idl}$ points to Q(x_0, y_0, z_0). By getting the $\boldsymbol{B_j}$ generated by the jth energized segment at Q, $\boldsymbol{E_j}$ can be calculated according to (1), and finally, $\boldsymbol{B}$ and $\boldsymbol{E}$ generated by the entire coil are obtained according to (5), where k represents the number of energized segments.

$$\boldsymbol{B} = \sum_{j=1}^{k} \boldsymbol{B}_j \qquad \boldsymbol{E} = \sum_{j=1}^{k} \boldsymbol{E}_j \tag{5}$$

The process of calculating the integral directly is complicated and easy to make mistakes. Use (6) to calculate B_x, B_y, and B_z separately and then sum the vectors to simplify the calculation.

$$\begin{cases} B_x = \dfrac{\mu_0 I}{4\pi}\left(\displaystyle\int_{y_1}^{y_2} \frac{z_0 - z}{r^3} dy - \int_{z_1}^{z_2} \frac{y_0 - y}{r^3} dz\right) \\ B_y = \dfrac{\mu_0 I}{4\pi}\left(\displaystyle\int_{z_1}^{z_2} \frac{x_0 - x}{r^3} dz - \int_{x_1}^{x_2} \frac{z_0 - z}{r^3} dx\right) \\ B_z = \dfrac{\mu_0 I}{4\pi}\left(\displaystyle\int_{x_1}^{x_2} \frac{y_0 - y}{r^3} dx - \int_{y_1}^{y_2} \frac{x_0 - x}{r^3} dy\right) \end{cases} \tag{6}$$

Taking the finite element solution as a reference to verify the correctness of EM-ACM, simulate the square coil in Comsol Multiphysics 6.1 [15], which is located in the xy plane at $z = 20$mm (Fig.1 a), set the excitation as $I = 1$A and $f = 1$Hz. According to (7), calculate the relative error of 26×26 observation points in the plane of $z = -15$mm, x, $y \in$[-25mm, 25mm], where X_a stands for EM-ACM value and X_s stands for finite element value.

$$\delta = \frac{X_a - X_s}{X_s} \tag{7}$$

As shown in Fig.1 b) and c), $\max|\delta_B| = 1.4618\%$, average $|\delta_B| = 0.2313\%$; $\max|\delta_E| = 0.4215\%$, average$|\delta_E| = 0.1511\%$. The field distribution obtained by the two methods is consistent, which proves the EM-ACM calculation results are accurate. Moreover, EM-ACM avoids the problems of long calculation time and the need for observation point spacing much smaller than the grid size in the finite element method.

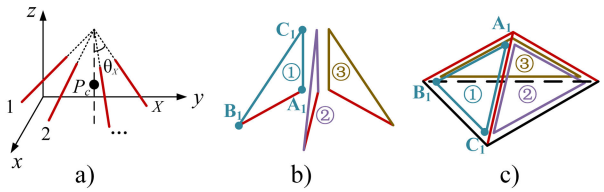

FIGURE 2. ①, ②, and ③ are coil numbers. a). Coil "skeleton" structure. b). Independent structure. c). Non-independent structure.

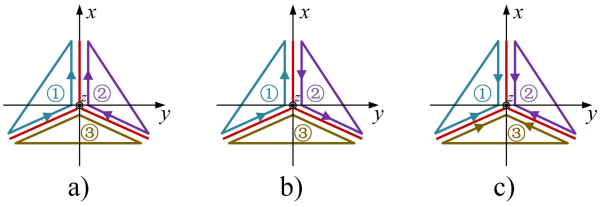

FIGURE 3. ①, ②, and ③ are coil numbers. The principle of Fig.2 c) structure (projected on the xy plane) generating electric field components. a). Generate E_x. b). Generate E_y. c). Generate E_z.

B. COIL DESIGN

In this paper, the electric field in different directions is realized by changing the ratio between E_x, E_y,and E_z, proposing the "skeleton" structure EC-X with controllable induction electric field direction based on the superposition principle (Fig.2 a), X represents the number of "mainly functional energized segment" (red line segment), only when X≥3 can achieve the control of electric field direction, and P_c is the stimulation target. To reduce the number of redundant energized segments, the "skeleton" is closed into the triangle. Taking EC-3 as an example, explain the reason for designing the "skeleton" structure (Fig.2 a) as independent (Fig.2 b) instead of non-independent (Fig.2 c).

The non-independent structure (Fig.2 c) generates E_x, E_y,and E_z, through the power modes shown in Fig.3, the coil loop restricts the current flow and cannot achieve Fig.3 c), which cannot only generate E_z. In addition, the real coil has certain width and thickness, and the non-independent structure (Fig.2 c) allows the winding to spread on the plane, increasing interference with target stimulation. As shown in Fig.2 b), in the independent structure, the "mainly functional energized segment" current direction does not interfere with each other and can generate E_z separately. In addition, A_nC_n and B_nC_n (n=1,2…X) are far away from the target, with less stimulation interference. Therefore, it is necessary to design the "skeleton" structure as an independent structure (Fig.2 b).

The independent structure (Fig.2 b) is referred to as EC-3, EC-3 consists of three identical isosceles triangles spaced 120° apart, reserving a gap in the middle to facilitate coil heat dissipation. The angle between coil ① and -y is 30°, the angle between coil ② and +y is 30°, and coil ③ is located

TABLE 1. EC-3 power modes.

Coil	Mode E_x	Mode E_y	Mode E_z	Mode E
①	$+I$	$-I$	$-I$	$-I$
②	$+I$	$+I$	$-I$	$+I$
③	$-2I$	0	$-I$	$-3I$
Outcome	E_x	E_y	E_z	E

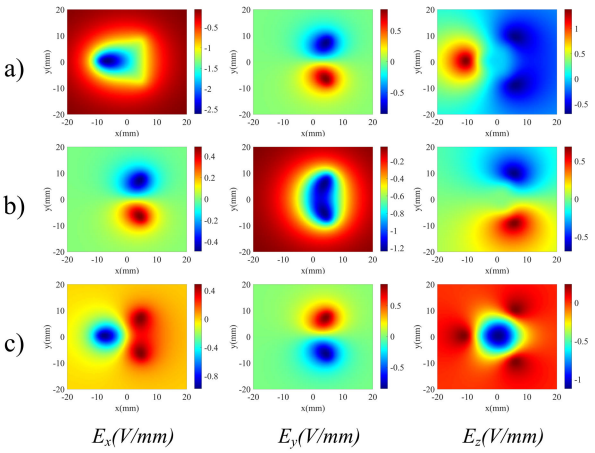

FIGURE 4. E_x, E_y, and E_z distribution in different modes. a). Mode E_x. b). Mode E_y. c). Mode E_z.

TABLE 2. EC-4 power modes.

Coil	Mode E_x	Mode E_y	Mode E_z	Mode E
①	$-2I$	0	$-I$	$-3I$
②	0	$+2I$	$-I$	$+I$
③	$+2I$	0	$-I$	$+I$
④	0	$-2I$	$-I$	$-3I$
Outcome	E_x	E_y	E_z	E

in the *xoz* plane (Fig.5 a). The proportion and direction of the coil current when EC-3 produces E_x, E_y,and E_z, are shown in Table 1, the current from A_n to B_n is $+I$.

Using EM-ACM calculates the distribution of electric field components in *xy* plane under different power modes in Table 1, set parameter conditions: $I = 1$A, $f = 2.5$kHz, $a = 10$mm, $\theta = 120°$ (Fig.2 c, a = length of A_nB_n, $\theta = \angle C_nA_nB_n$). As shown in Fig.4, at (x,y)=(0,0), Mode E_x can achieve $E_y = E_z = 0$, $E_x \neq 0$; Mode E_y can achieve $E_x = E_z = 0$, $E_y \neq 0$; Mode E_z can achieve $E_x = E_y = 0$, $E_z \neq 0$. The field distribution calculated by EC-ACM proves theoretically that EC-3 can realize controllable electric field direction.

EC-3 has a large deviation between the $\boldsymbol{E_{max}}$ point P_{max} and the electric field direction controllable point P_c under Mode E (Fig.5 b), and the energy utilization rate is low. Transforming EC-3 into EC-4 with 90° interval distribution (Fig.5 c), Table 2 (A_n to B_n is $+I$) shows the power modes for generating electric field components in EC-4, the position deviation between P_c and P_{max} is significantly reduced (Fig.5 d).

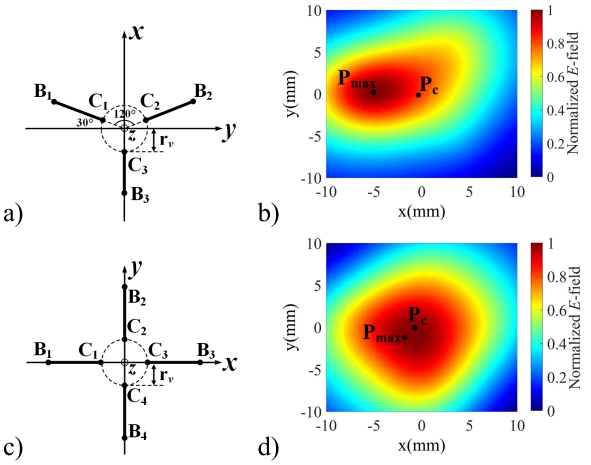

FIGURE 5. r_v is the cooling radius. a). EC-3 projected on the *xy* plane. b). Normalized E distribution of EC-4 in Mode E. c). EC-4 projected on the *xy* plane. d). Normalized E distribution of EC-4 in Mode E.

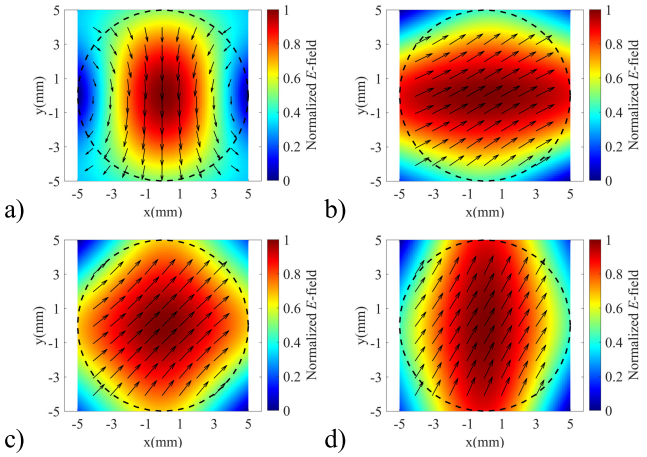

FIGURE 6. Normalized E distribution in the xy plane, with black arrows representing the direction of E and black dashed lines representing the rodent brain. a). Figure-8 coil. b). EC-4 synthesis 30°. c). EC-4 synthesis 45°. d). EC-4 synthesis 60°.

As shown in Fig.6 a), the ball head (dashed line) with a diameter of 10mm represents the rodent brain [16]. The 8mm diameter Figure-8 coil has a fixed electric field direction on the *xy* plane, it is necessary to adjust the coil to find the optimal stimulation direction when using. As shown in Fig.6 b), c), and d), EC-4 (A_nB_n = 8mm) can realize any direction of $\boldsymbol{E}$ on the plane, so it has a higher potential application.

III. COIL STRUCTURE OPTIMIZATION

A. OPTIMIZATION MODEL SIMPLIFICATION

The EC-X coil designed in this article aims to achieve controllable direction of the induced electric field. In practical use, it is expected that the controllable electric field direction point P_c will overlap with the stimulation target. Therefore, the electric field at P_c and its surrounding areas distribution requires special attention. The induced electric field spatial

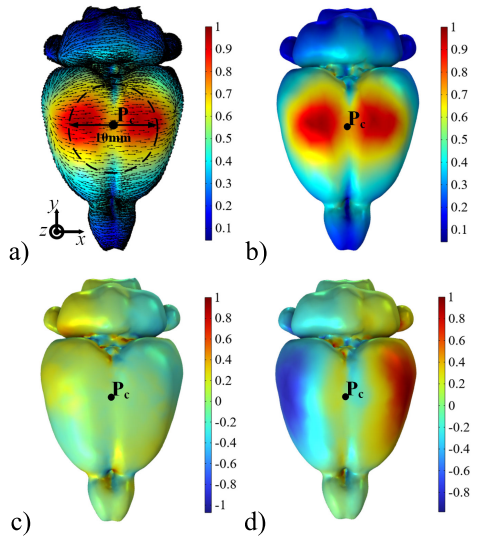

FIGURE 7. The normalized electric field distribution of the rat with real material properties. The black dotted line diameter is 10mm, P_c is the controllable electric field direction point, and the coil current ratio is 2:0:-2:0. a). E, the arrow represents the direction is $+x$. b). E_x. c). E_y. d). E_z.

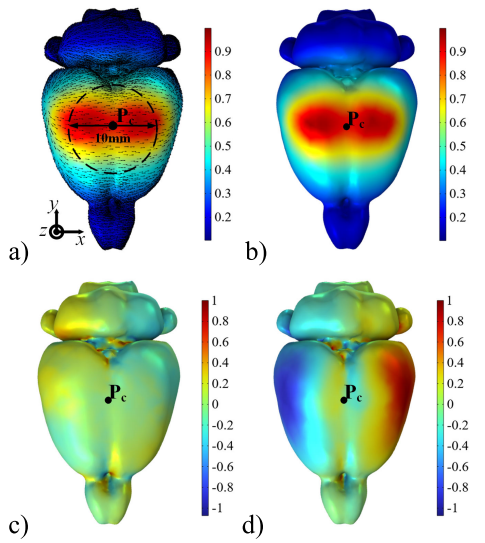

FIGURE 8. The normalized electric field distribution of the rat with air material properties. The black dotted line diameter is 10mm, P_c is the controllable electric field direction point, and the coil current ratio is 2:0:-2:0. a). E, the arrow represents the direction is $+x$. b). E_x. c). E_y. d). E_z.

distribution characteristics, such as stimulation intensity and focusing, can be improved by optimizing the coil structure and adjusting the relative position relationship between coil and stimulation target. According to the problem itself, we should optimize according to the real brain, but due to the geometric complexity and material nonuniformity, analytical calculations are difficult, and finite element analysis requires long time and high computational costs, so simplifying the optimization model and solving in the air domain. To ensure the effectiveness of the analytical results, we simulate the electric field distribution on the rat brain and verify that the electrification principle of EC-4 (see Table 2) is still applicable in vivo.

Firstly, refer to the atlas by RRID: SCR_017124, using Materialise Mimics (http://www.materialise.com) to process the MRI data of the Sprague Dawley Rat Brain [17], and complete the 3D model reconstruction. Then, perform smoothing and hole repair in Materialise 3-matic to generate the FEM model. Finally, simulate the distribution of electromagnetic fields in Comsol Multiphysics 6.1, set the parameter a = 8mm, $\theta = 130°$(a = length of A_nB_n, $\theta = \angle C_nA_nB_n$), the lowest point of the coil is 2mm above the surface of the brain, f = 2.5kHz, and is energized in Mode E_x. Since the finite element solver requires boundary surface closure, we concatenated the gray and white matter to generate a homogeneous rat model [18], the conductivity is 0.33 S/m.

For the convenience of comparing the distribution characteristics of induced electric field, the normalized distribution of electric field is shown in Fig.7. The surface electric field distribution is shown in Fig.7, the black dashed line depicts a circular area with diameter of 10mm centered on P_c (corresponding to MRI data 1:1, excluding the cerebellum and olfactory bulb). At the controllable electric field direction point P_c, $E_x \neq 0$, $E_y = E_z = 0$(Fig.7 b,c,d), similarly, Mode E_y and Mode E_z can respectively achieve $E_y \neq 0$ and $E_z \neq 0$. Fig.8 shows the electric field distribution of the rat brain with air material properties, which is basically consistent with the distribution in Fig.7, there is no significant change due to complex electromagnetic boundary conditions, indicating that optimizing the electric field distribution characteristics around P_c in air domain is effective. The simplified optimization model is shown in Fig.9 a).

B. OPTIMIZATION PROCESS

The ball head (R=5mm) is located below the coil (Fig.9 a), and ball center M(0,0,-9mm), target P_c(0,0,-7mm). When the coil structure changes, the coil always remains tangent to the ball head, the tangential distance is the material thickness d=4mm introduced by the coil support structure. With the change of coil structure parameters(a = length of A_nB_n, $\theta = \angle C_nA_nB_n$), the stimulation effect varies, as shown in Fig.9 b). Simplifying the coil into a line model, with a and θ as variables, finding the coil structure that is conducive to realizing any electric field direction is of great significance to improving stimulation efficiency. The stimulation efficiency is characterized by: i) maximum ampere-turn AN_{max}; ii) stimulation focusing degree F_c.

i) maximum ampere-turn AN_{max}

When the same structure (a,θ) generates omnidirectional $\boldsymbol{E_c}$ = 1V/m at P_c, the four coils of EC-4 require different total ampere-turn AN (Fig.9 d, a = 8mm, $\theta = 130°$). The maximum value of AN is AN_{max}, the smaller it is, the higher the energy utilization rate of this structure, and the more conducive to realizing any electric field direction.

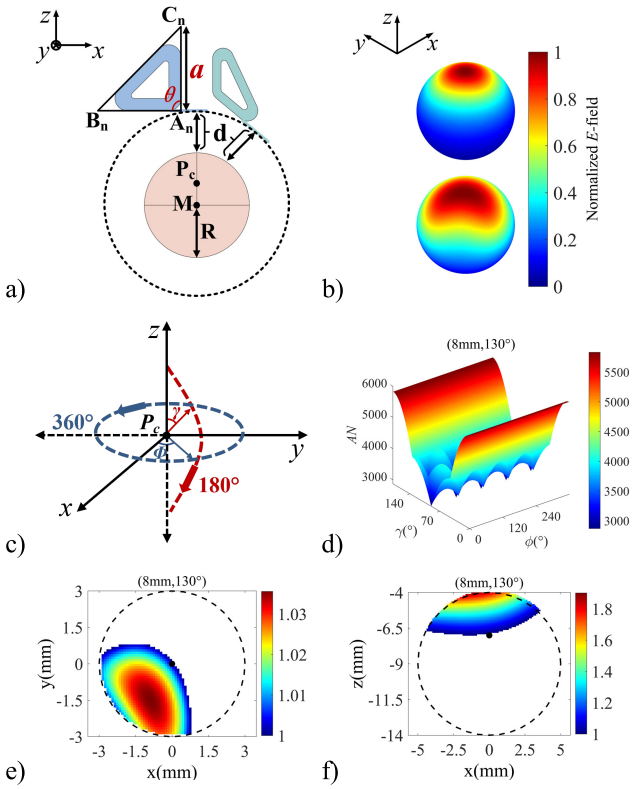

FIGURE 9. a). The position relationship between the ball head and the coil. b). (4mm,130°), (20mm,130°) structure, distribution of electric field acting on the ball head. c). Spherical coordinate, $\Phi \in [0°, 360°)$, $\gamma \in [0°, 180°]$. d). (8mm,130°) structure, the total number of ampere-turn required for four coils of EC-4 to generate an omnidirectional electric field(E_c =1V/m). e). (8mm,130°) structure, *xy* plane $E > E_c$ ($E_c = 1$) electric field distribution. f). (8mm,130°) structure, xz plane $E > E_c$ ($E_c = 1$) electric field distribution.

ii) stimulation focusing degree F_c

The controllable electric field direction point P_c is the actual application point, when analyzing the distribution characteristics of the induced electric field generated by EC-X, $\boldsymbol{E_c}$ at P_c is taken as the threshold, and the proportion of $\boldsymbol{E} > \boldsymbol{E_c}$ in the ball head is calculated to evaluate the stimulation focusing degree F_c. Directly calculating the volume ratio of the ball head introduces a large amount of calculation. For isotropic media, the electric field distribution in the volume model can be described by two-dimensional section, calculating the $\boldsymbol{E} > \boldsymbol{E_c}$ ($\boldsymbol{E_c} = 1$) distribution of P_c on the *xy* ($z = -7$mm) and *xz*($y = 0$mm) sections of the ball head using EM-ACM (Fig.9 e, f). Therefore, the area ratio of $\boldsymbol{E} > \boldsymbol{E_c}$ ($\boldsymbol{E_c} = 1$) is calculated through (8) to quantify the stimulation focusing degree F_c. The smaller the F_c, the higher the stimulation efficiency.

$$F_c = \frac{S_{E>E_c}}{S} \tag{8}$$

Follow the process shown in Fig.10 to optimize. Firstly, limit the range of a and θ. The closer the coil is to the target area($\theta \geq 90°$), the less energy is consumed, referring to the size of commercial animal coils [12], $a \leq 40$mm. In the

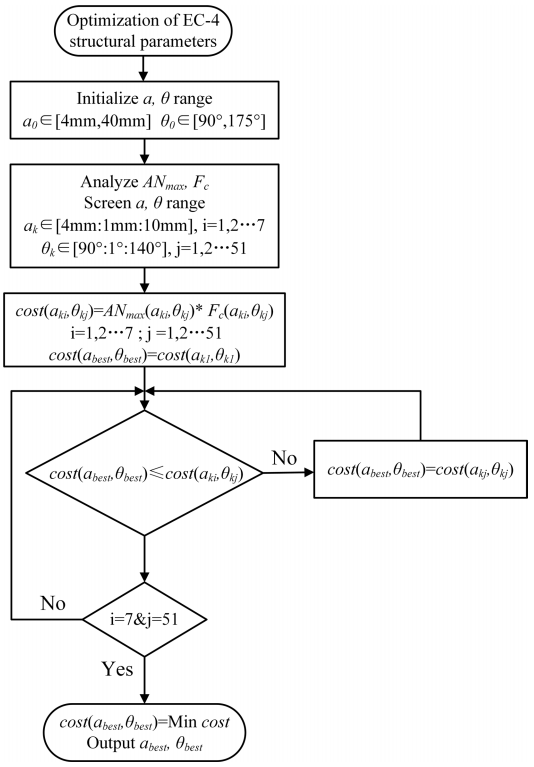

FIGURE 10. Coil structure optimization process.

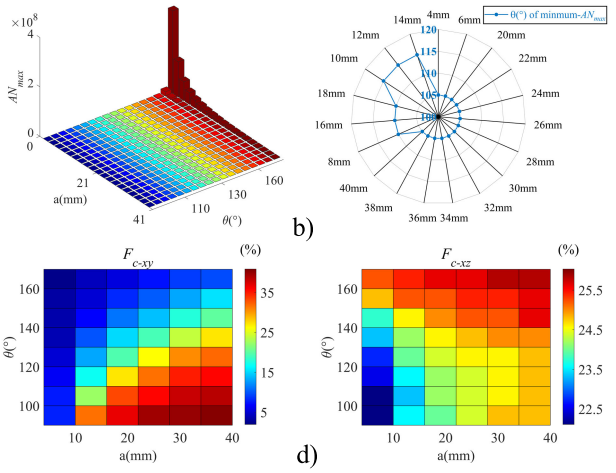

FIGURE 11. a). $\boldsymbol{AN_{max}}$ for different coil structures. b). θ at the minimum $\boldsymbol{AN_{max}}$ corresponding to different a. c). $\boldsymbol{F_{c-xy}}$ of the *xy* plane. d). $\boldsymbol{F_{c-xz}}$ of the *xz* plane.

triangle, when the radius of the inscribed circle is equal to the chamfer radius at the vertex angle, the triangle becomes circular. Due to process limitations, the chamfer radius of the coil winding column is about 0.4mm-0.5mm, and the inscribed circle radius greater than 1mm can better maintain the coil shape. Therefore, the initial range of the variable is limited to $a_0 \in [4\text{mm},40\text{mm}]$, $\theta_0 \in [90°,175°]$.

Discrete calculation AN_{max} at intervals of 2 mm and 5° in the range of a_0 and θ_0. Fig.11 a) shows the change rule

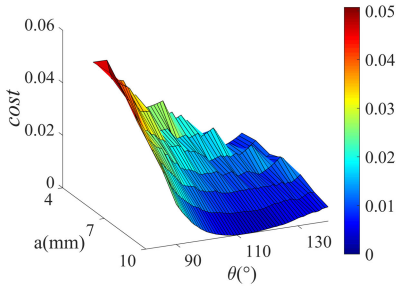

FIGURE 12. The cost under different structures.

of AN_{max}: for all θ, AN_{max} decreases monotonically as a increases; For all a, as θ increases, AN_{max} has a unique minimum point (Fig.11 b), and the value of θ is 105°, 110°, and 115°; $\theta > 140°$, AN_{max} begins to increase dramatically, and the larger θ is, the more drastic it becomes, resulting in significant increase in power consumption. Thus, θ has a constrained range of 90°-140°.

When the coil structure is transformed, the amount of calculation required to traverse the F_c of all electric field directions is very large. The ampere-turn ratio and geometric parameters (a and θ) of the EC-4 coil together determine the direction of $\boldsymbol{E}$ generated by the coil, under the same ampere-turn ratio, γ changes with a and θ, (φ, γ) is not unique, the optimization result is universal. Therefore, randomly select the ratio of ampere-turn -3:1:-1:-3, discrete calculation F_c at intervals of 6 mm and 10° in the range of a_0 and θ_0.

In the xy(z=-7mm) plane (Fig.11 c): the range of $F_{c-xy}$is 1.9%-40.8%; F_{c-xy} is inversely proportional to θ; F_{c-xy} is proportional to a, rapidly increasing within 4mm-6mm, a>10mm, slow growth of F_{c-xy}. In the xz(z=-7mm) plane (Fig.11 d): the range of F_{c-xz} is 22.1%-25.8%; F_{c-xz} is proportional to a and θ. The smaller F_c is, the more concentrated the stimulation is, F_{c-xy} and F_{c-xz} have obvious advantages within 10mm. Therefore, a has a constrained range of 4mm-10mm. In addition, the range of variation of F_{c-xy} is significantly larger than that of F_{c-xz}, only F_{c-xy} will be considered in subsequent analysis.

The influence of a on AN_{max} and F_{c-xy} is more significant than that of θ when the coil structure changes, increase in a, AN_{max} decrease, F_{c-xy} increase. Ideally, AN_{max} and F_{c-xy} should be as small as possible, comprehensively considering AN_{max} and F_{c-xy} define (9), the smaller the *cost*, the better. Based on the above analysis, further optimize the coil structure at intervals of 1mm and 1° in the range of $a_k \in$ [4mm,10mm] and $\theta_k \in$ [90°,140°], searching for a_{best}, θ_{best}. Before calculating *cost*, normalize AN_{max} and F_{c-xy} to avoid the influence of order of magnitude. As shown in Fig.12, the *cost* is the smallest at (10mm,113°) and (4mm,140°).

$$cost = AN_{\max} * F_{c-xy} \tag{9}$$

The above optimization is based on simplified line model, but the real coil has volume. In the application of TMS, the stimulation coil is connected to the circuit and powered by the control capacitor. The size and waveform of the coil current are related to the capacitor voltage U, capacitance C, coil resistance R, and inductance L. When designing the stimulus paradigm for specific diseases, it is necessary to adjust the coil structure according to the current waveform parameters to meet the requirements of R and L, a_{best} and θ_{best} are not unique. a>4mm, AN_{max} significant changes, causing *cost* to exhibit serrated changes near (4mm,140°); The *cost* varies smoothly and has a small value near (10mm,113°), show that the coil structure adjustment will not cause drastic changes in AN_{max} and F_{c-xy}. Thus, the geometric parameters of the coil are controlled within $a_{best} \in$ [8mm,10mm], $\theta_{best} \in$ [110°,120°], the stimulation is relatively concentrated and the energy utilization efficiency is high.

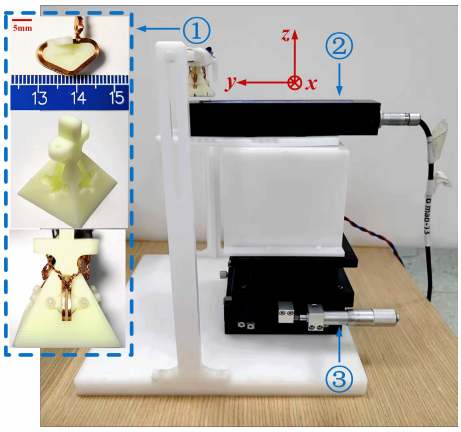

FIGURE 13. EC-4 coil and measurement platform. ① EC-4 coil. ② Mag-13 fluxgate sensor. ③ XYZ three-axis platform.

IV. EXPERIMENT

A. EC-4 COIL PHYSICAL OBJECT

$\boldsymbol{B}$ and $\boldsymbol{E}$ are coupled to each other, by measuring the distribution of $\boldsymbol{B}$, it can be indirectly verified that EC-4 can achieve controllable direction of $\boldsymbol{E}$. The current from A_n to B_n is $+I$, and the ampere-turn ratio is -3:1:-1:-3. According to the optimization results, use 1mm×0.1mm flat copper wire double-layer winding to produce two types of coils (spacing 0.8mm tough resin): 42 turns, $a_1 = 8.03$mm, $\theta_1 = 120°$; 14 turns, $a_2 = 10.34$mm, $\theta_2 = 120°$. The support structure using nylon resin 3D printing is a tetrahedral structure (Fig.13), insert the coil into the groove to meet the cooling radius $r_v \approx 1.5$mm.

B. MAGNETIC FIELD DISTRIBUTION MEASUREMENT EXPERIMENT

Measurement of $\boldsymbol{B}$ uses the Mag-13 fluxgate sensor, the excitation ($f = 7$Hz, $V_{pp} = 30$mV) is realized through the signal generator and the power amplifier. The XYZ three-axis platform is used to meet the measurement spatial resolution, which is made of alloy material and has an impact on the target measurement value, reducing the interference by raising the Mag-13.

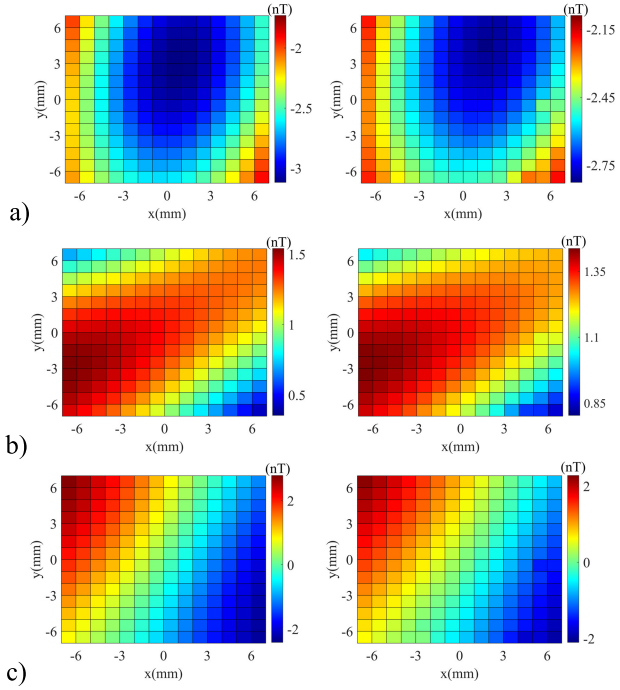

FIGURE 14. Magnetic field distribution, EM-ACM calculation values on the left, and experimental values on the right. a). B_x. b). B_y. c). B_z.

Positioning in the *xyz* direction is achieved through nylon material gantry, the origin is the intersection of the EC-4 central axis and the *xy* plane. The measuring plane is approximately 30mm away from the lowest point of the coil, and measurement range is $x, y \in$[-7mm,7mm], with resolution of 1mm and total of 225 points. The magnetic field distribution under 1mA excitation is shown in Fig.14. Measurement errors include various factors, such as difficult to determine machining errors in the winding part of the coil, positioning deviations due to high measurement resolution, and interference from the XYZ three-axis platform. The purpose of experiment is to observe the magnetic field distribution and not to analyze the errors between values. Comparing the experimental and EM-ACM calculation results, the magnetic field distribution is basically consistent. Based on the above analysis, EC-4 proposed in this paper can achieve controllable direction of electric field.

V. CONCLUSION

Animal TMS research is significant in advancing the development of human TMS, and the commonly used experimental subject is rat. The shape of the coil determines the distribution of the induced electric field, and its spatial resolution hinders the traceability of physiological experimental results. Considering the sensitivity of the TMS stimulation effect to the direction of the induced electric field, this paper proposes a coil structure that can control the direction of induced electric field to improve stimulation efficiency.

Firstly, establish the Electromagnetic field Analytical Calculation Model (EM-ACM) to analyze the distribution of $\boldsymbol{E}$ induced by coils, and verify its correctness through finite element simulation results. Any electric field direction is realized by controlling the proportion of E_x, E_y,and E_z, and the ''skeleton'' structure EC-X with controllable $\boldsymbol{E}$ is proposed. The EM-ACM proves that EC-3 can control the direction of electric field. Considering the energy utilization efficiency, EC-4 is chosen.

Next, in order to improve stimulation efficiency, EC-4 is simplified into a line model, with a and θ (a=length of A_nB_n, $\theta = \angle C_nA_nB_n$) used as variables to optimize the coil structure. The coil size control at $a_{best} \in$[8mm,10mm], $\theta_{best} \in [110°, 120°]$ is more friendly and can take into account both energy efficiency AN_{max} and stimulus focusing degree F_c.

Finally, measure the magnetic field distribution in the *xy* plane below the coil, experimental results are consistent with EM-ACM calculation. It proves the feasibility of the electric field direction controllable structure (EC-X) proposed in this paper from both theory and experiment.

In the mechanism research of TMS, cable theory provides theoretical framework for understanding how TMS-induced electric field polarizes and activates neurons [19]. Generally speaking, the neural response depends on the direction of the nerve relative to the electric field direction, due to the local variation of the effective conductivity component in the electric field direction, the sensitivity threshold of different types of neurons to the same electric field direction is different. The sensitivity threshold can be understood as the electric field intensity required to achieve suprathreshold stimulation in that electric field direction [20]. By searching for the direction of the electric field with the lowest sensitivity threshold for target neurons, the effective stimulation energy threshold can be reduced, and there is room to further reduce the interference to the nontarget area, thereby improving stimulation focality.

Most animal TMS coils are designed to control the amplitude distribution of $\boldsymbol{E}$, and focus is improved by combining shielding layers or iron core materials. When evaluating coil performance, the electric field amplitude is used to calculate focus and stimulation intensity, ignoring the direction of the electric field. Comparative analysis of the working principles of the two types of coils, it is not difficult to find that the direction of $\boldsymbol{E}$ generated by the Figure-8 coil on the plane below it is fixed, EC-X realizes the direction transformation of $\boldsymbol{E}$ by adjusting the ampere-turn ratio of the current flowing through the coil. When applying the coil, it is necessary to adjust the position and direction of the coil relative to the head, to change the direction of the electric field in the target area, which is inconvenient to operate. The EC-X coil proposed in this article has the characteristic of controllable electric field direction, by changing the proportion of current flowing into the coil, the electric field direction of the target area can be changed without moving the coil, providing a tool for finding the electric field direction with the lowest sensitivity threshold of the target area neurons.

This study mainly verifies the correctness of the controllable electric field direction principle realized by EC-X through simulation and experiment. When considering the

electric field direction, quantifying stimulus focality requires combining the electric field in anatomy with the real neurons in morphology. In future research, anisotropy in real models will be considered to more accurately evaluate the effect of EC-X coil.

ACKNOWLEDGMENT

This work was supported by the Space Environment Simulation Research Infrastructure (Space Magnetic Environment Simulation and Research System). The authors would like to thank the Frontiers Science Center for Matter Behave in Space Environment.

REFERENCES

[1] T. Wagner, J. Rushmore, U. Eden, and A. Valero-Cabre, "Biophysical foundations underlying TMS: Setting the stage for an effective use of neurostimulation in the cognitive neurosciences," *Cortex*, vol. 45, no. 9, pp. 1025–1034, Oct. 2009, doi: 10.1016/j.cortex.2008.10.002.

[2] Y. Roth, A. Amir, Y. Levkovitz, and A. Zangen, "Three-dimensional distribution of the electric field induced in the brain by transcranial magnetic stimulation using figure-8 and deep H-coils," *J. Clin. Neurophysiol.*, vol. 24, no. 1, pp. 31–38, Feb. 2007, doi: 10.1097/wnp.0b013e31802fa393.

[3] B. Sahin, H. Aslan, B. Unal, S. Canan, S. Bilgic, S. Kaplan, and L. Tumkaya, "Brain volumes of the Lamb, rat and bird do not show hemispheric asymmetry: A stereological study," *Image Anal. Stereol.*, vol. 20, no. 1, p. 9, May 2011, doi: 10.5566/ias.v20.p9-13.

[4] A. Luft, A. Kaelin-Lang, T.-K. Hauser, L. Cohen, N. Thakor, and D. Hanley, "Transcranial magnetic stimulation in the rat," *Exp. Brain Res.*, vol. 140, no. 1, pp. 112–121, Sep. 2001, doi: 10.1007/s002210100805.

[5] A. Rotenberg, P. A. Müller, A. M. Vahabzadeh-Hagh, X. Navarro, R. López-Vales, A. Pascual-Leone, and F. Jensen, "Lateralization of forelimb motor evoked potentials by transcranial magnetic stimulation in rats," *Clin. Neurophysiol.*, vol. 121, no. 1, pp. 104–108, Jan. 2010, doi: 10.1016/j.clinph.2009.09.008.

[6] A. D. Tang, A. S. Lowe, A. R. Garrett, R. Woodward, W. Bennett, A. J. Canty, M. I. Garry, M. R. Hinder, J. J. Summers, R. Gersner, A. Rotenberg, G. Thickbroom, J. Walton, and J. Rodger, "Construction and evaluation of rodent-specific rTMS coils," *Frontiers Neural Circuits*, vol. 10, Jun. 2016, doi: 10.3389/fncir.2016.00047.

[7] F. A. Khokhar, L. J. Voss, D. A. Steyn-Ross, and M. T. Wilson, "Design and demonstration in vitro of a mouse-specific transcranial magnetic stimulation coil," *IEEE Trans. Magn.*, vol. 57, no. 7, pp. 1–11, Jul. 2021, doi: 10.1109/TMAG.2021.3077976.

[8] T. Yoshikawa, H. Higuchi, R. Furukawa, and T. Tateno, "Temporal and spatial profiles of evoked activity induced by magnetic stimulation using millimeter-sized coils in the mouse auditory cortex in vivo," *Brain Res.*, vol. 1796, Dec. 2022, Art. no. 148092, doi: 10.1016/j.brainres.2022.148092.

[9] S. D. March, S. J. Stark, R. L. Hadimani, D. R. Stiner, M. J. Senter, K. K. Spoth, L. J. Crowther, and D. C. Jiles, "Thermal and mechanical analysis of novel transcranial magnetic stimulation coil for mice," *IEEE Trans. Magn.*, vol. 50, no. 9, pp. 1–5, Sep. 2014, doi: 10.1109/TMAG.2014.2316479.

[10] H. Yu, B. Du, L. Guo, and G. Xu, "Design of transcranial magnetic stimulation coils for mouse with improved stimulus focus and intensity," *IEEE Trans. Magn.*, vol. 58, no. 2, pp. 1–4, Feb. 2022, doi: 10.1109/TMAG.2021.3084451.

[11] K. R. Mills, S. J. Boniface, and M. Schubert, "Magnetic brain stimulation with a double coil: The importance of coil orientation," *Electroencephalogr. Clin. Neurophysiol./Evoked Potentials Sect.*, vol. 85, no. 1, pp. 17–21, Feb. 1992, doi: 10.1016/0168-5597(92)90096-t.

[12] R. Salvador and P. C. Miranda, "Transcranial magnetic stimulation of small animals: A modeling study of the influence of coil geometry, size and orientation," in *Proc. Annu. Int. Conf. IEEE Eng. Med. Biol. Soc.*, Sep. 2009, pp. 674–677, doi: 10.1109/IEMBS.2009.5334070.

[13] R. Salvador, S. Silva, P. J. Basser, and P. C. Miranda, "Determining which mechanisms lead to activation in the motor cortex: A modeling study of transcranial magnetic stimulation using realistic stimulus waveforms and sulcal geometry," *Clin. Neurophysiol.*, vol. 122, no. 4, pp. 748–758, Apr. 2011, doi: 10.1016/j.clinph.2010.09.022.

[14] B. J. Roth, J. M. Saypol, M. Hallett, and L. G. Cohen, "A theoretical calculation of the electric field induced in the cortex during magnetic stimulation," *Electroencephalogr. Clin. Neurophysiology/Evoked Potentials Sect.*, vol. 81, no. 1, pp. 47–56, Feb. 1991, doi: 10.1016/0168-5597(91)90103-5.

[15] *AC/DC Module User's Guide*, COMSOL AB, Stockholm, Sweden, 2021, pp. 75–84.

[16] L. Liu, M. Ding, J. Wu, Y. Zhang, S. Guo, N. Wang, H. Wang, K. Yu, Y. Weng, L. Luo, J. Zhang, Q. Zhang, K. Qiu, Y. Wu, X. Xiao, and Q. Zhang, "Design and evaluation of a rodent-specific focal transcranial magnetic stimulation coil with the custom shielding application in rats," *Frontiers Neurosci.*, vol. 17, Apr. 2023, Art. no. 1129590, doi: 10.3389/fnins.2023.1129590.

[17] E. A. Papp, T. B. Leergaard, E. Calabrese, G. A. Johnson, and J. G. Bjaalie, "Waxholm space atlas of the Sprague Dawley rat brain," *NeuroImage*, vol. 97, pp. 374–386, Aug. 2014, doi: 10.1016/j.neuroimage.2014.04.001.

[18] L. M. Koponen, M. Stenroos, J. O. Nieminen, K. Jokivarsi, O. Gröhn, and R. J. Ilmoniemi, "Individual head models for estimating the TMS-induced electric field in rat brain," *Sci. Rep.*, vol. 10, no. 1, p. 17397, Oct. 2020, doi: 10.1038/s41598-020-74431-z.

[19] H. R. Siebner et al., "Transcranial magnetic stimulation of the brain: What is stimulated? A consensus and critical position paper," *Clin. Neurophysiol.*, vol. 140, pp. 59–97, Aug. 2022, doi: 10.1016/j.clinph.2022.04.022.

[20] A. S. Aberra, B. Wang, W. M. Grill, and A. V. Peterchev, "Simulation of transcranial magnetic stimulation in head model with morphologically-realistic cortical neurons," *Brain Stimulation*, vol. 13, no. 1, pp. 175–189, Jan. 2020, doi: 10.1016/j.brs.2019.10.002.

JIAYU ZHAI received the B.E. degree in measurement and control technology and instruments from Hebei University, Baoding, China, in 2022. She is currently pursuing the M.E. degree in electrical engineering with Harbin Institute of Technology (HIT), Harbin, China. Her main research interest includes animal magnetic stimulation.

JINTING WANG received the B.E. degree in mechanical engineering from Northeastern University (NEU), Shenyang, China, in 2019, and the M.E. degree in mechanical engineering from Harbin Institute of Technology (HIT), Harbin, China, in 2021, where she is currently pursuing the Ph.D. degree in electrical engineering. Her main research interest includes the magnetic stimulation.

HAO CUI received the B.E. degree in electrical engineering from Harbin Institute of Technology (HIT), Harbin, China, in 2021, where he is currently pursuing the M.E. degree in electrical engineering. His main research interest includes biological magnetic stimulation.

QIMING CHEN (Member, IEEE) was born in Heilongjiang, China, in 1984. He received the B.E. degree from Harbin University of Science and Technology (HUST), Harbin, China, in 2007, the M.E. degree from Harbin Engineering University (HEU), Harbin, in 2010, and the Ph.D. degree from Harbin Institute of Technology (HIT), Harbin, in 2016.

Since 2020, he has been Associate Research Fellow with the Laboratory for Space Environment and Physical Sciences, HIT. His research interests include high power converters and multilevel converters.

JIUGE LIN is currently pursuing the B.E. degree in electrical engineering with Harbin Institute of Technology (HIT), Harbin, China. Her main research interests include transcranial magnetic stimulation and neurophysics.

DONGHUA PAN (Member, IEEE) received the B.E. and M.E. degrees in electrical engineering from Shenyang University of Technology, Shenyang, China, in 2005 and 2008, respectively, and the Ph.D. degree in electrical engineering from Harbin Institute of Technology (HIT), Harbin, China, in 2013.

Since 2020, he has been a Professor with the Laboratory for Space Environment and Physical Sciences and the Department of Electrical Engineering, HIT. His main research interests include zero magnetic field facility, weak magnetic field environment application, and detection of weak magnetic information.

LIYI LI (Member, IEEE) received the B.E. degree in instrument science and technology, the M.E. degree in mechanical engineering, and the Ph.D. degree in electrical engineering from HIT, Harbin, China, in 1991, 1995, and 2001, respectively.

Since 2004, he has been a Professor with the Laboratory for Space Environment and Physical Sciences and the Department of Electrical Engineering, HIT. He has authored or coauthored more than 151 technical articles and is the holder of 80 patents. His research interests include zero magnetic field facility, control and drive of linear motors, and superconducting motors.